Plasma Sci. Technol. **20** (2018) 014010 (7pp) https://doi.org/10.1088/2058-6272/aa8c6f

Optical measurements and analytical modeling of magnetic field generated in a dieletric target

Yafeng BAI (白亚锋)[1,2,5], **Shiyi ZHOU** (周诗怡)[2,5], **Yushan ZENG** (曾雨珊)[2], **Yihan LIANG** (梁亦寒)[3], **Rong QI** (齐荣)[2], **Wentao LI** (李文涛)[2], **Ye TIAN** (田野)[2,6], **Xiaoya LI** (李晓亚)[3] **and Jiansheng LIU** (刘建胜)[2,4,6]

[1] MOE Key Laboratory of Advanced Micro-structured Materials, Institute of Precision Optical Engineering, School of Physics Science and Engineering, Tongji University, Shanghai 200092, People's Republic of China
[2] State Key Laboratory of High Field Laser Physics, Shanghai Institute of Optics and Fine Mechanics, Chinese Academy of Sciences, Shanghai 201800, People's Republic of China
[3] National Key Laboratory of Shock Wave and Detonation Physics, China Academy of Engineering Physics, Mianyang 621000, People's Republic of China
[4] IFSA Collaborative Innovation Center, Shanghai Jiao Tong University, Shanghai 200240, People's Republic of China

E-mail: tianye@siom.ac.cn and michaeljs_liu@siom.ac.cn

Received 12 July 2017, revised 11 September 2017
Accepted for publication 13 September 2017
Published 28 November 2017

Abstract

Polarization rotation of a probe pulse by the target is observed with the Faraday rotation method in the interaction of an intense laser pulse with a solid target. The rotation of the polarization plane of the probe pulse may result from a combined action of fused silica and diffused electrons. After the irradiation of the main pulse, the rotation angle changed significantly and lasted ~2 ps. These phenomena may imply a persistent magnetic field inside the target. An analytical model is developed to explain the experimental observation. The model indicates that a strong toroidal magnetic field is induced by an energetic electron beam. Meanwhile, an ionization channel is observed in the shadowgraph and extends at the speed of light after the irradiation of the main beam. The formation of this ionization channel is complex, and a simple explanation is given.

Keywords: magnetic field, faraday rotation, ionization channel

(Some figures may appear in colour only in the online journal)

1. Introduction

The interaction of ultra-intense, ultra-short laser pulses with a solid target is at the very basis of fast ignition [1], astrophysics [2], proton and ion acceleration [3, 4], and so on [5–7]. In fast ignition, of particular interest are the megaampere currents of relativistic electrons that propagate into the target [8]. These currents can generate megagauss magnetic fields, which will in turn influence the propagation of the energetic electron beam, thereby diminishing the energy deposition in the precompressed ignition core. As electrons penetrate into the target, a low-energy electron backflow will be generated in order to ensure electric neutrality [9]. In such a system Weibel instability [10] or the current filamentation instability can grow efficiently and give rise to an ultra-intense magnetic field in a manner that is akin to the formation of an ultraintense magnetic field from unmagnetized plasmas in astrophysics [11]. In this way, the Weibel instability renders the laser–solid interaction an excellent test field for astrophysics [12].

The temporal evolution of multimegagauss magnetic fields is dictated by many different mechanisms. In the

[5] These authors contributed equally to this work.
[6] Authors to whom any correspondence should be addressed.

penetration phase of fast electrons into a target, the magnetic field is mainly determined by the source term $\nabla \times (\eta j_b)$ [13], where j_b is the beam current density, and η is the electric resistivity. When η is assumed to be a constant, the magnetic field is mainly determined by j_b. The magnetic field can also grow at points where there is a gradient in the electric resistivity $\nabla\eta$ that is not aligned with the energetic electron current j_b. On the other hand, in addition to the current of fast electrons generated during the interaction, the crossed density and temperature gradients $\nabla n \times \nabla T$ and the temporal variations in the ponderomotive force are also responsible for causing the intense magnetic field. Haines in [14] incorporated all mechanisms above into one equation.

Recording and investigating the magnetic field is complicated. Various methods have been developed for detecting the magnetic field, including the magnetic probe, current probes, Zeeman effect [15], plasma polarimetry [16], and proton probe [11, 17], to name a few. The most effective way to date is plasma polarimetry based on the magneto-optic Faraday Effect and the Cotton–Mouton effect. The Faraday Effect was used in [18–21] to detect the magnetic field in front of the target or in an underdense plasma. The Cotton–Mouton effect is capable of detecting the temporal evolution of the magnetic field near the critical surface of the plasma [22–27]. Progress has been made in observing the Weibel-like instability induced turbulent magnetic field [24]. The magnetic field has also been observed at the rear side of the target [23]. Moreover, methods that employ the polarization properties of high order harmonics of the laser frequency are utilized to detect magnetic fields near the critical density [28, 29]. Nonetheless, despite diverse detecting methods, the study of the magnetic field induced in the interaction of the laser light with a solid is not sufficient. The theoretical prediction of intense magnetic field inside the target lacks of experimental validation.

In this paper, we show the temporal evolution and space distribution of a Multi-Megagauss toroidal magnetic field utilizing the Faraday rotation method. An analytical model is developed to explain the experimental observation and it yields calculation results in good agreement with the experiment. After irradiation of the main beam, an ionization channel is observed, which is attributed to the filament of the laser light in the target. In addition, we observed a weak magnetic field near the ionization channel. This may indicate the presence of an electron beam.

2. Experimental setup

The experiment was performed at a commercial 1 kHz Ti: sapphire femtosecond laser facility, which produces 25 fs, 8 mJ pulses with a central wavelength of 800 nm at a maximum repetition rate of 1 kHz. The experimental arrangement is shown in figure 1(a). The 800 nm laser beam was focused with an $f/2$ off-axis parabola at normal incidence onto a fused silica target coated with a 50 μm thick film. At the best focus, the p-polarized beam was focused to a 5 μm diameter spot, producing a maximum irradiance of about 1×10^{17} W cm^{-2}. Targets were located in a vacuum chamber. The probing beam was obtained by splitting off a small fraction of the incident light, frequency-doubled to the ultraviolet range (400 nm), and used as probes for time-resolved polarimetry and plasma shadowgraphy. The probe beam passed transversely across the target front surface. The spatial resolution of the shadowgraphy was designed to be approximately 2 μm. The probe beam was synchronized by decreasing the relative delay to a value, at which no plasma was detected in the diagnostics, that was defined as zero time.

The main laser pulse is always preceded by a low-intensity, long-duration pedestal (∼ns) that is introduced by amplified spontaneous emission as well as the imperfect compression of the chirped pulse. With an intensity of $\sim 1 \times 10^{15}$ W cm^{-2}, it is sufficient to produce a preplasma in front of the target. Later, as the critical surface moves away from the ablation front, the main laser–plasma interaction takes place in this preplasma. The adjustment of the envelope of the pedestal preceding the main laser pulse was accomplished by altering the timing of optical gates in the laser chain. Figure 1(b) presents such envelope of the laser pulse.

Polarimetry relies on the polarization rotation of the probe pulse. It is essentially the Faraday Effect caused by the magnetic field component parallel to the propagation direction of the probe pulse. Thus the rotation angle φ_{tot} of the linear polarized probe pulse presents a direct measure of the magnitude of the magnetic field [15]. The time evolution of the magnetic field can also be determined from polarimetry.

3. Experimental results

To show the experimental results concisely, figure 2 presents typical polarigrams taken before illumination of the main beam (at time zero). The fringes are due to diffraction in the steep density profile. Specifically, (a)–(c) display the target picture when the Glan prism in front of the CCD was rotated away from the extinction of the original probe beam polarization by $\theta_{pol} = 90°$, 0°, and 5°, respectively. The polarigram shown in figure 2(a) shows no difference from that taken without the interaction of a laser beam. While at the same time delay, in figure 2(b), two bright spots were observed in the target where crossed polarizers were used. This demonstrates that the polarization planes of the two bright spots are rotated away from its original direction. To determine its polarization, we rotated the polarizer, and the intensity of the bright spots changed as the Glan polarizer was rotated. The intensities of the upper bright spot recorded at time delay zero at different θ_{pol} on the CCD are listed in table 1. Meanwhile, the results calculated with the Malus's Law are also shown in the table. Considering the fact that the interaction of laser light with solid target is a very unstable process, φ_{tot} should fluctuate from shot to shot. The data shown in table 1 demonstrate that the experimental results to a great extent obey Malus's law. Thus, it is reasonable to say the upper bright spot is linearly polarized. The fact that these two bright spots maintained linear polarization indicates a rotation of the polarization plane of the probe pulse by the target. In figure 2(c), an up-down asymmetry in the lighted

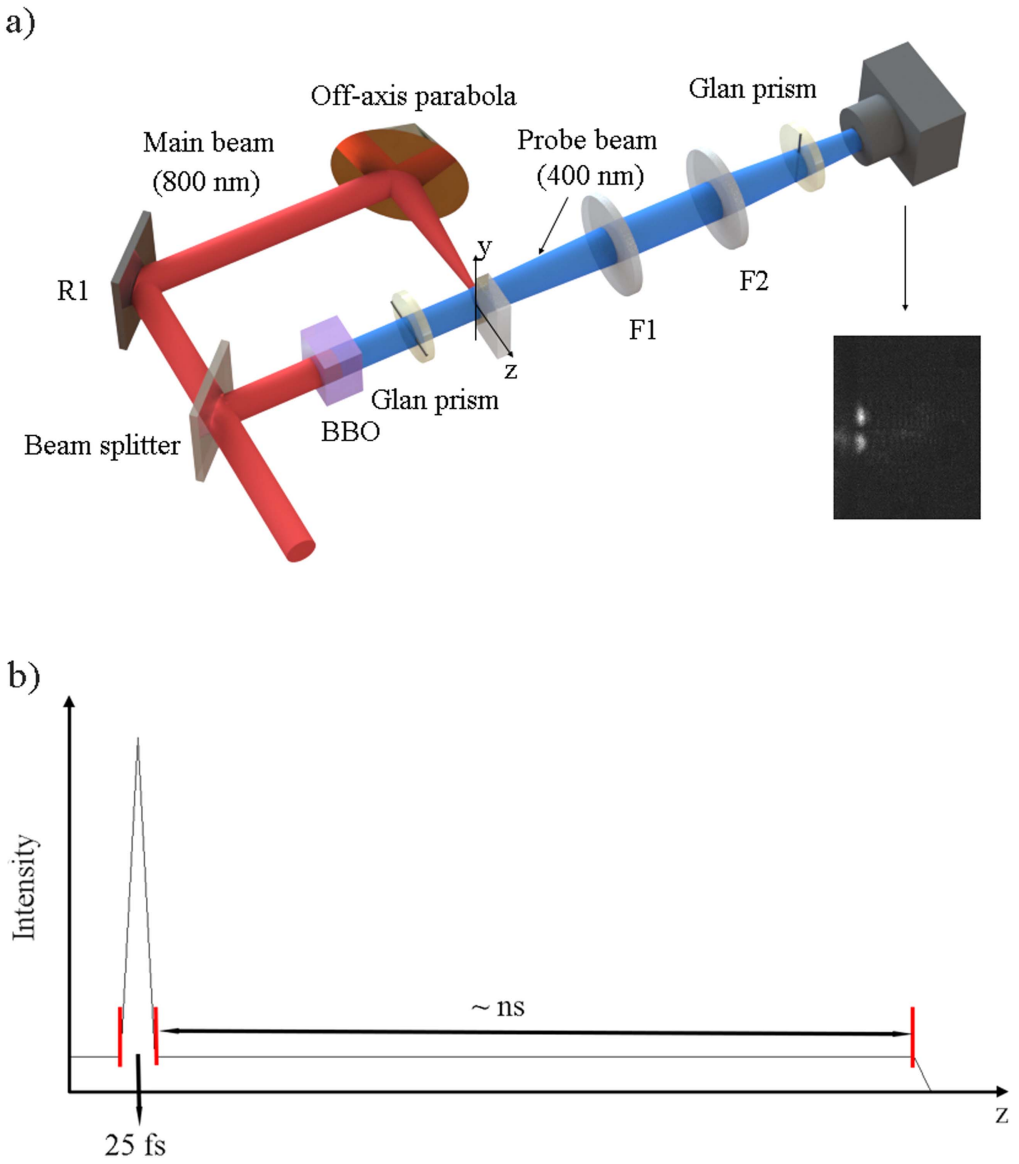

Figure 1. (a) Polarimetry diagnostic setup. The target surface is coated with a 50 μm thick Al film. The corresponding y and z directions are marked in the figure. (b) A sketch diagram for the laser pulse with a preceding pedestal.

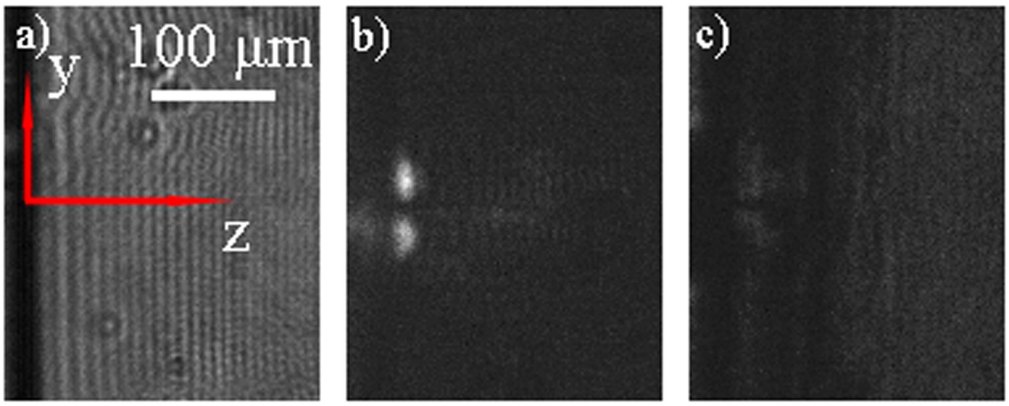

Figure 2. Polarigrams of the target taken before the illumination of the main beam when the Glan prism in front of a CCD was rotated away from the extinction of the original probe beam polarization by (a) 90°, (b) 0°, and (c) 5°. The corresponding coordinate system is shown in (a).

Table 1. Intensity of the upper bright spot recorded on CCD when the Glan polarizer is rotated away from the extinction position at different angles θ_{pol}($I_{laser} \sim 2072$, $\varphi_{tot} \sim 4°$, background noise is subtracted from the data below, at time delay zero).

θ_{pol} (degree)	$-10°$	5°	10°
Intensity (a.u.)	28	54	134
$I_{laser}\sin^2(\theta_{pol} + \varphi_{tot})$ (a.u.)	22	52	122

pattern is observed. This indicates that the two bright spots in figure 2(b) are in different polarization states, demonstrating an azimuthal magnetic field in the target. This effect is most obvious when θ_{pol} is near the rotation angle φ_{tot} of the polarization plane of the probe pulse. Thus it can be estimated that at time delay zero, φ_{tot} is approximately around 5°. In order to get the rotation angle of the incident light, we rotate the polarizer until the background signal in the CCD is comparable to that of the lighted region and the rotation angle can be estimated. The rotation angle can also be estimated by Malus's law. If the intensity of the background signal recorded in the CCD is I_{bg} and the intensity of the spot is I_{sp}, then

$$I_{sp} = I_{bg}\sin^2(\phi_{rot} + \theta_{pol}). \tag{1}$$

The rotation angles from the two methods are consistent. With this method, the time evolution of the rotation angle is measured and is shown in figure 3(a). As shown in the picture, the rotation angle fluctuated around a stable value until the illumination of the main pulse. Once the heating beam was on (namely, after time zero) the rotation angle changed tremendously as it increased to a value of ~11°. This phenomenon may hint on an increment of the magnetic field inside the target. The rotation angle decreased soon after the main heating pulse and lasted ~3 ps.

In contrast to the experiments in [18, 19] where the spatial and temporal evolution of the spontaneous magnetic field were studied in front of the target, our experiment observed the Faraday rotation inside the target. However, the complex environment inside the target complicates the process of retrieving magnetic field from the rotation angle. As laser light energy is absorbed and reflected from the target, some portions are transformed into the energy of the electron that is transmitted into the target and thereby heats the target. The electron density inside the target is estimated to be $<10^{18}\,\mathrm{cm}^{-3}$. For a probe pulse that propagates in a plasma along the magnetic-field force lines, the rotation angle is proportional to the integral, taken along the path L, of the product of the electron density n_e by the longitudinal component $B\|$ of the magnetic induction vector:

$$\phi_{rote} = \frac{en_e}{2m_e cn_c}B_{\|}L, \tag{2}$$

where n_c is the critical density corresponding to the probe pulse. For $L \sim 60\ \mu$m and a rotation angle of 11°, this yields a magnetic field of $\sim 110^9$ G, which is unreasonable for our experimental parameters. The rotation of the polarization plane of the probe pulse may be attributed to a different mechanism. It should be noticed that the target is composed of fused silica, and the Faraday effect was first discovered by Michael Faraday in 1845 in glass. The rotation of the polarization plane of the probe pulse may result from a combined action of the fused silica and the diffused electrons. The relation between the angle of rotation of the polarization plane and the magnetic field in a glass is

$$\phi_{rotg} = \frac{1}{2}\frac{eB_{\|}L}{m_e c}\lambda\frac{\mathrm{d}n}{\mathrm{d}\lambda} = VB_{\|}L, \tag{3}$$

where n is the refractive index of the glass, and V is the temperature dependent Verdet constant. The temperature of the ionized electron inside the target can range from several eV to keV [30, 31]. However, the solid target will enter unstable state picoseconds after the interaction of the laser beam with the target. Whereas the temperature of the electrons is high, the unionized fused silica may not. In our case, the ionization ratio of the glass is <1‰. Determining the temperature of the unionized fused silica is not easy. Here, we suggest a rather simple model to estimate the temperature of the unionized target. It is reasonable to assume that a 5% laser energy deposition (which equals to ~0.4 mJ) is translated into the temperature increment of the unionized target. Suppose the two bright spots are approximately a $100\ \mu\mathrm{m} \times 100\ \mu\mathrm{m} \times 100\ \mu\mathrm{m}$ cubic. Taking into consideration the density $\sim 2.203 \times 10^3\,\mathrm{kg\,m^{-3}}$ and heat capacity $\sim 670\,\mathrm{J\,kg^{-1}\,°C}$ of the fused silica, the temperature raised by the heating pulse is estimated to be ~270 °C, which is much lower than that of the hot electrons. Therefore, we can reasonably assume that the target is not excited. However, the temperature distribution is not even. As shown in figure 2(b), the dark area in the middle of the two bright spots is assumed to be the axis of the toroidal magnetic field. The total angle of rotation of the polarization plane can thus be written as:

$$\phi_{rot} = \phi_{rotg} + \phi_{rote} = \left(V + \frac{en_e}{2m_e cn_c}\right)B_{\|}L. \tag{4}$$

For the fused silica used in our experiment, $V \sim 6.1\,\mathrm{deg\,cm^{-1}\cdot T^{-1}}$, and $\frac{en_e}{2m_e cn_c} \sim 3 \times 10^{-3}\,\mathrm{deg\,cm^{-1}\cdot T^{-1}}$, which is much smaller than the Verdet constant of fused silica and will be neglected in the following analysis. The temperature dependence of the Verdet constant is on the order of $10^{-4}\,\mathrm{K^{-1}}$ [32]. Thus, it is reasonable that we use a value of $7\,\mathrm{deg\,cm^{-1}\cdot T^{-1}}$ to retrieve the magnetic field from the rotation angle of the polarization plane of the probe pulse.

4. Analytical model for experimental observation

Figure 3(b) presents the temporal evolution of the magnetic field. It indicates a main pulse generated magnetic field pulse with a peak value of ~2 MG and duration of 2 ps (FWHM). As mentioned above, the generation of an intense magnetic field is a complex process for which various models have been developed while attempting to explain experimental observations [14]. The process involves numerous mechanisms such as the propagation of hot electrons inside a target, and misalignment between the pressure gradient and the density gradient. In order to analyze the underlying physical mechanisms of the experimental result, a very simple model is developed to simulate the space distribution and time

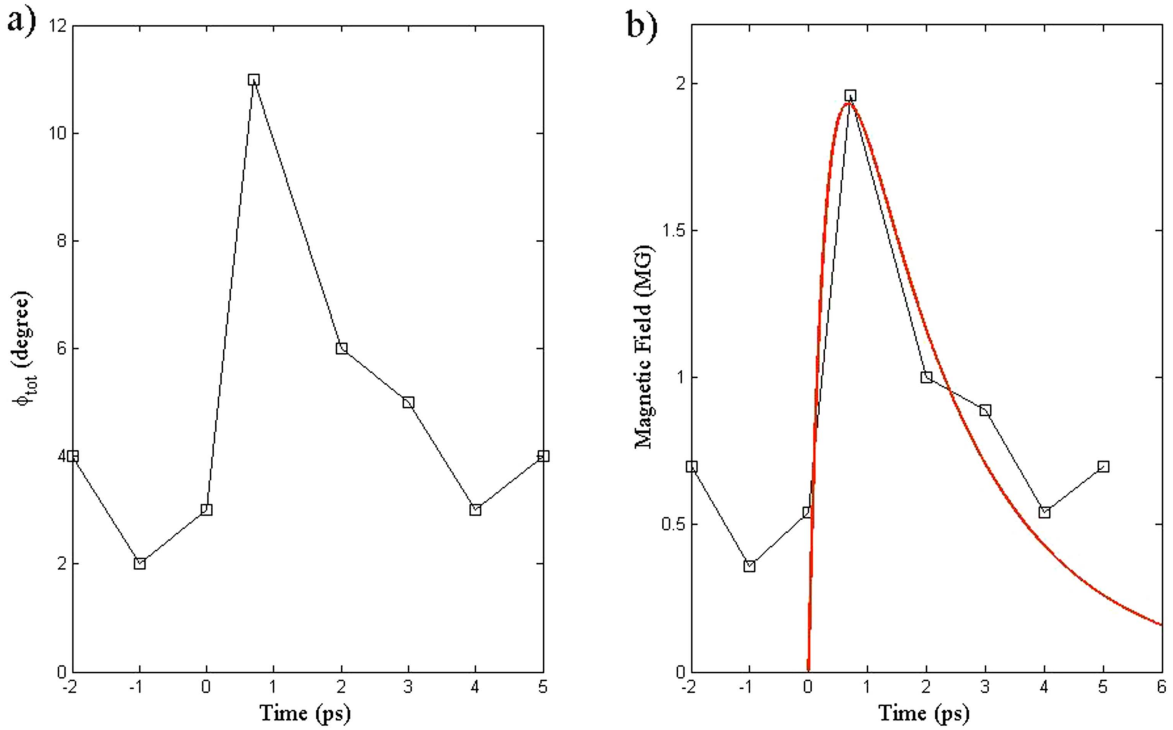

Figure 3. (a) Probing beam rotation angle φ_{tot} as a function of delay time; (b) magnetic field pulse profile retrieved from (a). Red solid line shows the fit obtained using electron current modeling.

evolution of the magnetic field induced by the main heating beam. The time evolution of the quasistatic magnetic field is determined by Faraday's law. By using Ohm's law, the equation for the magnetic field can be written as [25]

$$\frac{\partial \vec{B}}{\partial t} = \frac{c}{n_e e}\nabla T_e \times \nabla n_e + \frac{c}{\sigma_c}\nabla \times \vec{j}_{hot} + \frac{c^2}{4\pi\sigma_c}\nabla^2 \vec{B}, \quad (5)$$

where T_e is the temperature of the electron beam, n_e is the number density of the electron beam and j_{hot} is its current density. σ_c is the conductivity of the target. However, the first term on the right side of the equation is negligible for our experimental parameters. By approximating ∇T_e with $\Delta T_e/\Delta r_T$ and ∇n_e with $\Delta n_e/\Delta r_n$, and setting $\Delta T_e \sim 50\,\mathrm{eV}$, $\Delta n_e \sim 10^{18}/\mathrm{cm}^3$, $\Delta r_T \sim 50\,\mu\mathrm{m}$, and $\Delta r_e \sim 10\,\mu\mathrm{m}$, this gives $\partial B/\partial t = 10^{-3}\,\mathrm{MG\,ps}^{-1}$, a value much smaller than the experimental results. Therefore, the contribution of this source term can be neglected in the following analysis, which yields contributions only from the hot electron source term and the magnetic diffusion term. Whereas hot electrons are the main source for the intense magnetic field, the magnetic diffusion term results from the plasma return current and is representative of the resistive decay of the magnetic field. The current carried by the fast electrons can be estimated to be $\sim e\sigma n_e v_f$, where e is the elementary charge, σ is the cross-sectional area of the current, and v_f is the velocity of the fast electrons. After the irradiation of the main beam on the target, a typical parameter is $n_e \sim 1\times10^{18}\,\mathrm{cm}^{-3}$, and $v_f \sim 0.6c$, where c is the velocity of light in vacuum. If this current were to enter the target as a cylinder-shaped moving electron beam with radius $r_{spot} \sim 18\,\mu$m, the peak magnetic field under this condition gives $\mu_0 e n_e v_f r_{spot}/4 \sim 2.1$ MG, a result consistent with the experimental observation. However, this current cylinder has a limited length penetration depth L. Then the energy in the magnetic field would be of the order of $\pi r_{spot}^2 LB^2 \ln(L/r_{spot})/\mu_0$, which can be greater than the energy of the laser pulse for a large L. This implies a balancing return current induced by the hot electrons. This prediction is consistent with the experimental results: the fact that the two experimentally observed bright spots appear only in vicinity of the target front surface, or in other words, they never penetrate deep into the target, may indicate the place where an intense magnetic field is present, and thus the presence of net current. To validate our assumption, a model is developed as follows, taking the assumptions above to reproduce the space distribution of the magnetic field. The current density near the target front surface is assumed to be

$$j(r,z) = \frac{I_0 \exp\left(-\dfrac{z^2}{2\Gamma^2}\right)}{2\pi r_{spot}^2}\exp\left(-\frac{r^2}{2r_{spot}^2}\right), \quad (6)$$

where $r = \sqrt{x^2+y^2}$, Γ is a parameter used to characterize the return current effect determined by the magnetic diffusion term and the corresponding coordinate system is shown in figure 2. Though j is dependent on z, only an azimuthally magnetic field is detectable in the experiment. Thus, the current can be seen as a cylinder, and the azimuthal magnetic

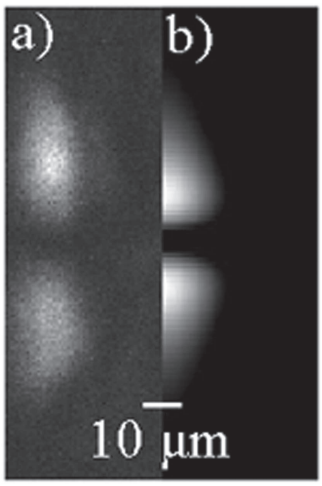

Figure 4. (a) Faraday rotation image in crossed polarizers, and (b) corresponding absolute value of magnetic field $|B(r, z)|$ calculated with equation (7).

field at (R, Z) is calculated to be

$$B(R, Z) = 2 \times 10^{-7} I_0 \exp\left(-\frac{z^2}{2\Gamma^2}\right) \frac{1 - \exp\left(-\dfrac{R^2}{2r_{\text{spot}}^2}\right)}{R}(T). \tag{7}$$

To compare with the results of the experiment, $|B(r, z)|$ is calculated when $I_0 = e\sigma n_e v_f = 2\,\text{kA}$, and $\Gamma = 10\,\mu\text{m}$, and is shown in figure 4(b), which has a two bright spots structure similar to that in figure 4(a). This consistency confirms the cylinder current assumption. On the other hand, time evolution of the magnetic field is of great significance [24] in addition to the space distribution. The time evolution of the magnetic field can be derived from equation (5). It is not easy to solve equation (5) directly without approximation. As indicated in [25, 26], $\nabla^2\vec{B}$ can be approximated with $B/\Delta r^2$, while $\nabla \times \vec{j}_{\text{hot}}$ can be approximated with $j_{\text{hot}}/\Delta r$. Since ultrashort laser beam was used in experiment and we only care about the transport of the energetic electron beam after the laser pulse, j_{hot} must decay over time. However, it is not easy to derive an explicit expression for j_{hot}. A model for the electron beam density is derived in [33] and used in [26] to obtain the expression for the magnetic field. Nonetheless, a simpler model developed in [25] is more suitable for uncovering the underlying physics. With this simpler model, electron current decay over time is modeled with an exponential function, and the final expression for the magnetic field is

$$B(t) = A\mu \exp\left(-\frac{t}{t_0}\right)\left[1 - \exp\left(-\frac{t}{\mu}\right)\right], \tag{8}$$

where $\mu = \dfrac{t_0\tau}{t_0 - \tau}$, $\tau = \dfrac{4\pi\sigma}{c^2}(\Delta r)^2$, and A is a source term. It can easily be seen when $t \gg \mu$, $B(t) \sim A\mu \exp(-t/t_0)$, and when $t \sim 0$, $B(t) \sim A\mu[1 - \exp(-t/\mu)]$. Thus μ determines the rising time of the magnetic field, while t_0 determines the falling time. For $\tau \gg t_0$, $\mu \sim \tau$. The peak value can be deduced to be $A\mu\left[\left(\dfrac{\tau}{t_0}\right)^{\frac{\mu}{t_0}} - \left(\dfrac{\tau}{t_0}\right)^{\frac{\mu}{\tau}}\right]$ at $t = \ln(t_0/\tau)/\mu$. Fitting the experimental result with this function can determine A, t_0, and τ. For the best fit curve shown in figure 3(b), the relevant parameters for the fused silica are $A = 9\,\text{MG ps}^{-1}$, $t_0 = 0.3\,\text{ps}$, and $\tau = 2\,\text{ps}$. The conductivity σ, which determines the decay time constant τ can be calculated to be $\sim 3.6 \times 10^{13}\,\text{s}^{-1}$. At a low temperature, glass is regarded as almost nonconducting [26]. Interestingly, because of the preionization of the target by the preceding pedestal in our experiment, a nonzero value is observed. Meanwhile, heating of the target with the conllisional effects as well as ionization via large electric fields exceeding the breakdown threshold can also contribute to this experimental result [26]. The space distribution and the time evolution of the magnetic field can be written as one equation:

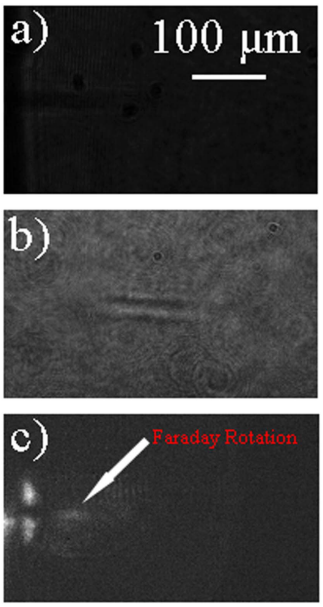

Figure 5. Shadowgraphic images of (a) the target, (b) a laser beam filament in the air at 2 ps after the main laser pulse irradiates the target, and (c) Faraday rotation image of the target at the same time delay of (a).

$$B(r, z, t) = 2 \times 10^{-7} A_0 \mu I_0 \exp\left(-\frac{z^2}{2\Gamma^2}\right)\exp\left(-\frac{t}{t_0}\right) \times \frac{\left[1 - \exp\left(-\dfrac{r2}{2r_{\text{spot}}^2}\right)\right]\left[1 - \exp\left(-\dfrac{t}{\mu}\right)\right]}{R}(T). \tag{9}$$

Here, A_0 is a constant.

5. Ionization channel in the target

In addition to an intense magnetic field, we also experimentally obtained an ionization channel extended with the speed of light after the interaction of the main beam with the target.

Figure 5(a) shows a characteristic shadowgraph of the ionization channel. Similar result has been observed in [34], and due to its small divergence angle and low extending speed ($\sim 0.66c$), this ionization channel was regarded to be excited by an energetic electron beam. However, the structure resembles to a greater extent the filament of a laser beam in glass, and the low extending speed $0.66c \sim \sqrt{2}c$ may result from an incident angle of 45°. The propagation of the laser beam in this ionization channel can be analyzed with the paraxial approximation [35, 36]. To corroborate this conjecture, we resort to a filament zone in air, as shown in figure 5(b). Owning to the filamentation of the laser light in air, the plasma zone appears as a dark line with a small divergence angle. The similarities between these two scenarios confirm our assumption. In some shots, the polarigrams of the target show a rather weak (that is, fluctuated around zero) magnetic field inside the ionization channel (see figure 5(c)). This may be attributed to the energetic electron beam induced by the laser light inside the ionization channel. It further confirms our assumption that the ionization channel is induced by the main heating beam rather than an energetic beam, because there should be an intense magnetic field around the ionization channel if it is raised by energetic electron beam. The ionization channel in air lasts approximately ~ 1 ns, while it is sustained for only about ~ 10 ps in glass. This could be a consequence of the enormous difference between the thermal conductivity of the two materials (air 0.023 W mK^{-1} glass 0.77 W mK^{-1} in room temperature). With regard to the contrast ratio of laser systems, it is regarded in [34] as a vital parameter for the observation of this ionization channel. In a low-contrast laser system, the preceding pedestal of the beam will preheat the target and introduce preplasma in front of the target. If this pre-pulse is strong enough, the main heating beam will be reflected and partly absorbed at the critical-density surface of the preplasma, thus allowing only the propagation of energetic electron beams into the target, where a dark ionization area appears. However, in the case of a high-contrast laser system, the pre-plasma is incapable of reflecting the main beam. The main beam penetrates into the target and forms filament in it, resulting in an ionization channel in the target.

6. Conclusion

We observed the characteristics of polarization rotation by a dielectric target in the interaction of a laser beam with a solid target. Two bright spots were obvious in the polarigrams and indicate a toroidal magnetic field. The magnetic field varies with time, and the rotation angle of the polarization plane may result from a combined action of the fused silica and the diffused electrons. An analytical model developed here shows good agreement with the experimental results. An ionization channel extending at the speed of light was also observed after the interaction of the main beam. This ionization channel is induced by the main beam. The magnetic field inside the ionization channel indicates a forward-propagating electron beam.

Acknowledgments

This work was supported by National Natural Science Foundation of China (Grant Nos. 11425418, 11405244, 1127901 and 61521093), the Strategic Priority Research Program (B) (Grant No. XDB16), and the Open Foundation of the National Key Laboratory of Shock Wave and Detonation Physics.

References

[1] Tabak M *et al* 1994 *Phys. Plasmas* **1** 1626
[2] Schoeffler K M *et al* 2016 *Phys. Plasmas* **23** 056304
[3] Maksimchuk A *et al* 2000 *Phys. Rev. Lett.* **84** 4108
[4] Wagner F *et al* 2016 *High Power Laser Sci. Eng.* **4** e45
[5] Nakajima K, Kim H T, Jeong T M and Nam C H 2015 *High Power Laser Sci. Eng.* **3** e10
[6] Lalousis P, Hora H and Moustaizis S 2014 *Laser Part. Beams* **32** 409
[7] Hora H *et al* 2015 *Laser Part. Beams* **33** 607
[8] Edwards C B and Danson C N 2015 *High Power Laser Sci. Eng.* **3** e4
[9] Smalyuk V A *et al* 2015 *High Power Laser Sci. Eng.* **3** e17
[10] Weibel E S 1959 *Phys. Rev.* **114** 18
[11] Huntington C M *et al* 2015 *Nat. Phys.* **11** 173
[12] Feilu Wang *et al* 2016 *High Power Laser Sci. Eng.* **4** e27
[13] Gremillet L, Bonnaud G and Amiranoff F 2002 *Phys. Plasmas* **9** 941
[14] Haines M G 1986 *Can. J. Phys.* **64** 912
[15] Pisarczyk T *et al* 1990 *J. Russ. Laser Res.* **11** 1
[16] Segre S E 1995 *Phys. Plasmas* **2** 2908
[17] Xing Zhang *et al* 2015 *High Power Laser Sci. Eng.* **3** e28
[18] Stamper J A and Ripin B H 1975 *Phys. Rev. Lett.* **34** 138
[19] Borghesi M *et al* 1998 *Phys. Rev. Lett.* **81** 112
[20] Najmudin Z *et al* 2001 *Phys. Rev. Lett.* **87** 215004
[21] Pisarczyk T *et al* 2015 *Phys. Plasmas* **22** 102706
[22] Shaikh M *et al* 2016 *Plasma Phys. Control. Fusion* **59** 014007
[23] Chatterjee G *et al* 2014 *Rev. Sci. Instrum.* **85** 013505
[24] Mondal S *et al* 2012 *Proc. Natl Acad. Sci.* **109** 8011
[25] Sandhu A S *et al* 2002 *Phys. Rev. Lett.* **89** 225002
[26] Sandhu A S *et al* 2006 *Phys. Rev.* E **73** 036409
[27] Kahaly S *et al* 2009 *Phys. Plasmas* **16** 043114
[28] Wagner U *et al* 2004 *Phys. Rev.* E **70** 026401
[29] Tatarakis M *et al* 2002 *Phys. Plasmas* **9** 2244
[30] Sarkisov G S *et al* 2012 *Phys. Rev.* E **86** 036412
[31] Gremillet L *et al* 1999 *Phys. Rev. Lett.* **83** 5015
[32] Williams P A *et al* 1991 *Appl. Opt.* **30** 1176
[33] Bell A R *et al* 1997 *Plasma Phys. Control. Fusion* **39** 653
[34] Dey I *et al* 2016 *Opt. Express* **24** 28419
[35] Castillo R, Ghatak A K and Hora H 1984 *Appl. Sci. Res.* **41** 359
[36] Osman F and Hora H 2000 *Laser Part. Beams* **18** 73